



Science Arts & Métiers (SAM)

is an open access repository that collects the work of Arts et Métiers ParisTech researchers and makes it freely available over the web where possible.

This is an author-deposited version published in: <http://sam.ensam.eu>
Handle ID: <http://hdl.handle.net/10985/8548>

To cite this version :

Christophe GIRAUD-AUDINE, F GIRAUD, M AMBERG, B LEMAIRE-SEMAIL - Vector control method applied to a traveling wave in a finite beam - Ultrasonics, Ferroelectrics, and Frequency Control, IEEE Transactions on - Vol. 61, n°1, p.147-158 - 2014

Any correspondence concerning this service should be sent to the repository

Administrator : archiveouverte@ensam.eu

Vector Control Method Applied to a Traveling Wave in a Finite Beam

Frédéric Giraud, *Member, IEEE*, Christophe Giraud-Audine, *Member, IEEE*, Michel Amberg, and Betty Lemaire-Semail, *Member, IEEE*

Abstract—This paper presents the closed-loop control of exciters to produce a traveling wave in a finite beam. This control is based on a dynamical modeling of the system established in a rotating reference frame. This method allows dynamic and independent control of the phase and amplitude of two vibration modes. The condition to obtain the traveling wave is written in this rotating frame, and requires having two vibration modes with the same amplitude, and imposing a phase shift of 90° between them. The advantage of the method is that it allows easy implementation of a closed loop control that can handle parameter drift of the system, after a temperature rise, for example.

The modeling is compared with measurement on an experimental test bench which also implements real-time control. We managed to experimentally obtain a settling time of 250 ms for the traveling wave, and a standing wave ratio (SWR) of 1.3.

I. INTRODUCTION

RESEARCHERS have devised many applications for high-frequency traveling waves. For example, they can convey a small carriage over a stator rail in a linear motor [1]–[3]. In that case, the elliptical motion of the vibrating stator drives the mechanical load directly, which is a simple solution compared with a rotary-to-linear movement transformation stage. They also can be used in peristaltic pumps [4] because the traveling wave micropumps are then free of rubbing parts. A traveling wave in a small cylindrical tube can also be obtained, and Sun *et al.* [5] used a combination of radial and axial modes of the tube, with specific driving conditions.

In general, the mechanical arrangement of such systems is quite simple. In fact, two exciters are used, one produces the vibration and the other absorbs the reflected wave. By swapping the role of the two exciters, a traveling wave in the reverse direction is obtained. However, to realize this, some conditions must be fulfilled, or no traveling wave propagates. These conditions have been studied in many papers. For example, Kuribayashi [6] described a

methodology to design the system, to choose the beam length and where to place the exciters on the beam. He also connected a resistor to the second exciter to dissipate the energy of the propagated wave. However, the practical realization of this solution suffers from poor efficiency, because a large amount of energy is lost into the resistor.

Therefore, some authors prefer an active sink instead [7]. In that case, the tuning of the exciters—their supply voltage, frequency and phase shift—becomes complex to obtain the traveling wave. The analytical solutions for a traveling wave in a string, a beam, and a membrane are given in [8]; the authors calculate the analytical expression of the applied forces to obtain a pure traveling wave in an undamped medium. They also show that it is sufficient to excite ten modes only; the other modes' contribution can be neglected. In [9], Dehez *et al.* proposed an optimization procedure. For their study, they first choose two neighboring vibration modes, which should be prominent. Then, they calculate the participation factors of a finite number of vibration modes *above* the chosen ones. They adjust their parameters through an optimization loop so as to make those factors as close as possible to those of the Fourier series coefficients of a square wave. In [10], Minikes *et al.* developed methods for identification and tuning of the traveling wave, or for multiple traveling waves [11]. They used a sensor array to measure the deformation amplitude and phase at specific points, then, an ellipse is fitted to the graph in the complex plane. If a pure traveling wave is obtained, then the fitted ellipse becomes a circle. Once again, they adjust the values of the excitation parameters through an online optimization process to reach the ideal case.

These methods can be off-line [8], [9], which means that the excitation is calculated before the experimental runs, or on-line [10] and can thus adapt themselves to variation in the operating conditions. However, their tuning procedure is based on steady states, and dynamic performances are not studied.

The method presented in this paper proposes to dynamically tune the two exciters to obtain a traveling wave in a slightly damped beam. The control algorithm relies on a model which is obtained from the theory of vibration in a beam, and which is detailed in the first section of this paper. After having verified this model through an experimental study, we establish this model in a rotating reference frame, to obtain constant-state variables at steady state. A specific closed-loop control is then deduced for our application, the performances of which are experimentally verified.

Manuscript received May 10, 2013; accepted September 26, 2013. This work was carried out within the framework of the Stintac Project of the Institut de Recherche sur les Composants logiciel et matériels pour la Communication Avancée (IRCICA), and the Mint team of INRIA Lille Nord-Europe.

F. Giraud, M. Amberg, and B. Lemaire-Semail are with the Institut de Recherche sur les Composants logiciels et matériels pour l'Information et la Communication Avancée (IRCICA), Université Lille 1, Villeneuve d'Ascq, France (e-mail: frederic.giraud@polytech-lille.fr).

C. Giraud-Audine is with the Ecole Nationale Supérieure d'Arts et Métiers, Villeneuve d'Ascq, France.

DOI <http://dx.doi.org/10.1109/TUFFC.2014.2885>

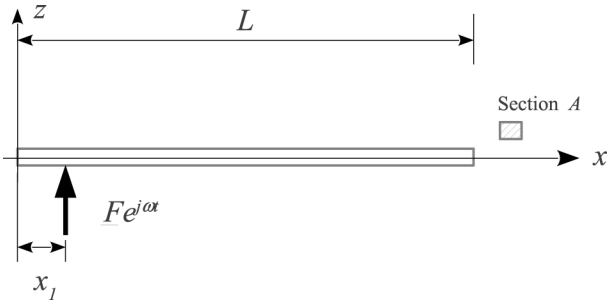


Fig. 1. The studied beam is supposed to be free at its ends and a sinusoidal load $\underline{F}(t)$ is applied at $x = x_1$.

II. BEAM THEORY

A. Mode Shape

In this study, we consider the forced vibration of the finite beam shown in Fig. 1. The transverse vibration of a uniform elastic homogeneous isotropic Euler–Bernoulli beam is described by the following differential equation [12]:

$$EI \frac{\partial^4 w}{\partial x^4} + \rho A \frac{\partial^2 w}{\partial t^2} + r_a \frac{\partial w}{\partial t} = p(x, t), \quad (1)$$

where E is the Young's modulus of the beam, I is the quadratic momentum of the beam, A is the cross section and ρ is the mass per unit volume of the beam, r_a is a coefficient of the external damping, $w(x)$ is the beam's deflection at point x and time t , and $p(x, t)$ is the load per unit length.

With a pure harmonic and concentrated excitation, the load p is written as $p(x, t) = \underline{F}\delta(x - x_1)e^{j\omega t}$, where $\delta(x)$ is the Dirac's delta function and $j^2 = -1$. The deflection is then considered as purely harmonic, and if we introduce \underline{w} such that w is the real part of \underline{w} , we can write

$$\underline{w}(x, t) = \underline{W}(t)\Phi(x)e^{j\omega t}. \quad (2)$$

In (2), \underline{W} includes both amplitude and phase of the deflection of the vibration. We should note that although ω is constant in the study, $\underline{W}(t)$ may vary with time. Thus, we not only consider the steady operation, but the transient as well. Moreover, \underline{w} is given for the deformation shape of the vibration $\Phi(x)$ which is normalized. Eq. (3) shows an example of a condition of normalization of the mode shape:

$$\int_0^L \rho A \Phi(x)^2 dx = 1. \quad (3)$$

The solution of (1) can be found in [9], [12], and will not be discussed in this paper. We note however, that we can analytically calculate the deflection for a particular position, as presented in Fig. 2. In this figure, we depict the deflection calculated at $x = 0.29$ m for an aluminum beam of 6×6 mm cross section and with $L = 0.48$ m. We also

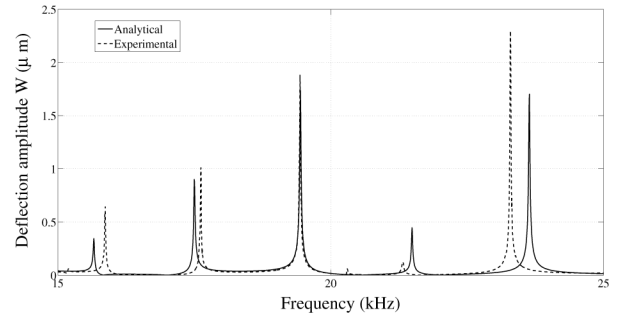


Fig. 2. Deflection amplitude as a function of frequency at $x = 0.29$ m with $x_1 = 0.196$ m and $L = 0.48$ m; comparison with experiment.

depict the experimental response of the beam, which is measured with a laser interferometer.

The analytical and experimental responses do not exactly match, despite some parameter adaptation done for this figure. This is mainly due to the analytical modeling, which considers an Euler–Bernoulli beam, which is not completely verified. However, differences are acceptable within the scope of this paper, because the proposed control doesn't require accurate parameter estimation. Furthermore, we show that beam's deflection has maximum values for particular excitation frequencies. These frequencies are known as eigenfrequencies, for which the beam has a specific shape, the so-called normal mode or modal shape. These deformation mode shapes refer to the function $\Phi_n(x)$, and they can be found either from analytical study, or more conveniently, from finite element modeling. Fig. 3 presents the deformation mode shapes for the two modes at 17500 and 19440 Hz (analytical).

Actually, under normal load excitation, every vibration mode is excited in the beam, but with different deflection, namely W_n . Eq. (2) is, in fact, an approximation of the beam's deflection around the vibration modes, and must be changed to

$$\underline{w}(x, t) = \sum_{n=1}^{\infty} W_n \Phi_n(x) e^{j\omega t}. \quad (4)$$

The deflection W_n depends on frequency. For example, they are maximal for the eigenfrequency ω_{0n} and the deformation which is then obtained corresponds to the func-

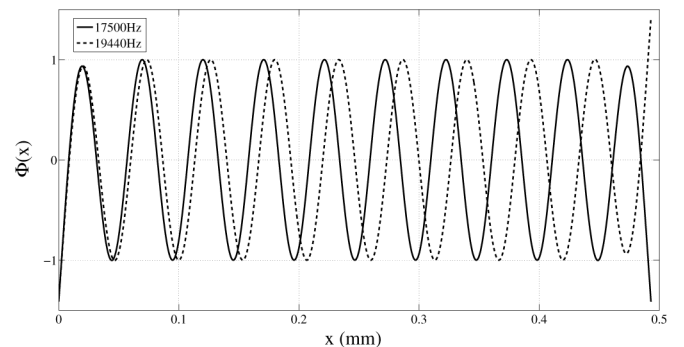


Fig. 3. Calculated deformation mode shape $\Phi(x)$ at 17500 and 19440 Hz.

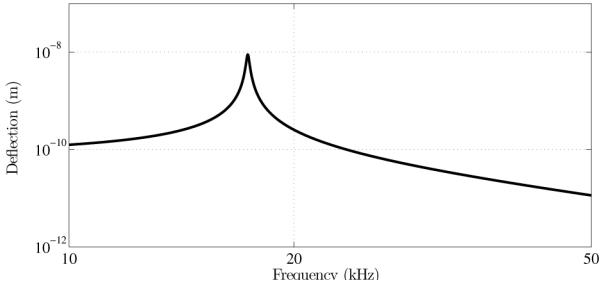


Fig. 4. Calculated deformation W_n as a function of frequency for the mode at 19440 Hz.

tion $\Phi_n(x)$. Fig. 4 shows the deflection W_n for the mode at 19440 Hz. As can be seen, this deflection follows the frequency response of a resonating low-pass filter: it is almost constant for $\omega < \omega_{0n}$ and then drops to 0 for $\omega > \omega_{0n}$.

Hence, the participation of a mode to the deformation of a beam is dominant if the working frequency is close to the eigenfrequency of this mode (i.e., $\omega = \omega_{0n}$), significant if the working frequency is lower than this eigenfrequency (i.e., $\omega < \omega_{0n}$), and negligible for working frequencies above the eigenfrequency (i.e., $\omega > \omega_{0n}$). This property is important and will be used later in this paper.

B. Conditions to Obtain a Traveling Wave

To produce a traveling wave, a second exciter is placed on the beam at distance x_2 . This configuration is described in Fig. 5.

Under certain supply conditions of the two exciters, it is possible to obtain a traveling wave. These conditions include adequately choosing the supply pulsation ω and the two forces F_1 and F_2 .

In principle, the idea is to use two neighbor modes a and b and to excite these two modes simultaneously, but shifted in time by 90° . In fact, when we consider the two deformation shapes in Fig. 3, we observe that they are close to sinusoidal shapes, and that they are almost space shifted by 90° , roughly in the region 0.2 m to 0.3 m in the middle. This condition can lead to a traveling wave, as presented in [10]. To obtain the two modes, we choose ω between the two eigenfrequencies: the lower mode is not too attenuated, whereas the higher one is significant.

These two modes are necessary, but not sufficient. In fact, we observe in the same Fig. 3 that the two modes are not phase shifted by 90° near the end of the beam. Consequently, if they were alone, they would not produce any traveling wave in that region. However, experimental studies in literature reported a traveling wave between the two exciters, and not only in the middle of the beam. This consideration illustrates the effect of the modes *above* the two chosen ones. Dehez *et al.* [9] have shown that they have influence in the ends and not in the middle of the beam. In this paper, we will consider that if the two modes a and b have the same amplitude and are phase shifted by 90° ($W_a = jW_b$), a traveling wave in the beam results. However, Gabai and Bucher [8] point out that perfect

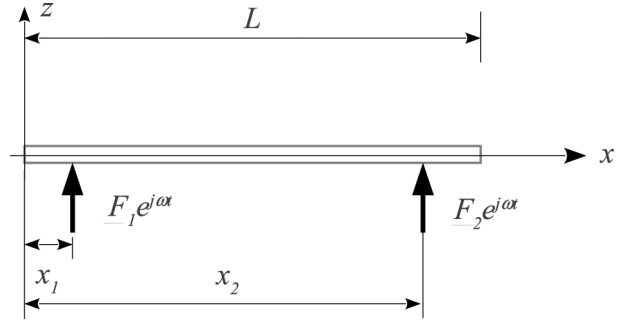


Fig. 5. The beam and its exciters to produce a traveling wave.

traveling wave is obtained when a large number of modes is taken into account; then, we expect to have an imperfect traveling wave in our case. This point will be quantified by experimental tests.

Studies reported in the bibliography do not control the two modes a and b directly: F_1 and F_2 are tuned until a perfect traveling wave is obtained, through an optimization algorithm, for instance. In this paper, we propose a method to directly control the two vibrations of the two modes a and b . This control relies on a model which is first presented, and then the control scheme is deduced and implemented on an experimental test bench.

III. DYNAMIC MODELING OF THE BEAM

The purpose of this section is to propose a model which allows us to calculate the evolution of the vibration amplitude of the modes a and b , and the phase shift between the two modes. In this section, we first apply beam theory to obtain a model which is confirmed by simulation results.

A. Modeling in a Fixed Reference Frame

This section deals with the evolution of the instantaneous vibration amplitude for the two modes. For that purpose, let $w_k(t) = W_k(t)e^{j\omega t}$, with $k = \{a, b\}$. This is equivalent to considering $w_k(t)$ as a rotating vector in a fixed frame, as depicted in Fig. 6. The length of this vector is $|W_k|$, and the projection on the real axis is the actual value which can be measured experimentally. Finally, the difference of the arguments of $W_k(t)$ represents the phase shift between the modes.

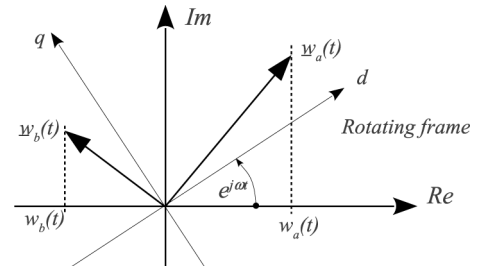


Fig. 6. Representation in a fixed reference frame.

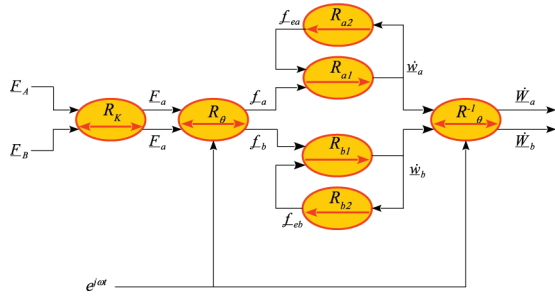


Fig. 7. The causal ordering graph of the system. 

Projecting (4) onto each mode [13], we obtain

$$\int_0^L EI \Phi_k(x) \frac{d^4 \Phi_k(x)}{dx^4} dx \underline{w}_k(t) + r_a \int_0^L \Phi_k^2(x) dx \underline{w}_k + \rho A \int_0^L \phi_k^2(x) dx \underline{w}_k = \int_0^L \Phi_k(x) p(x, t) dx, \quad k \in \{a, b\}. \quad (5)$$

For sake of simplification, we define:

- the modal mass $m_k = \rho A \int_0^L \Phi_k^2(x) dx$,
- the modal damping $d_{sk} = r_a \int_0^L \phi_k^2(x) dx$, and
- the modal stiffness $c_k = EI \int_0^L \Phi_k(x) ((d^4 \Phi_k(x)) / (dx^4)) dx$.

The participation K_{a1} and K_{a2} of each force F_1 and F_2 for mode a are defined as

$$\begin{aligned} \int_0^L \Phi_a(x) p(x, t) dx &= \Phi_a(x_1) \underline{F}_1 e^{j\omega t} + \Phi_a(x_2) \underline{F}_2 e^{j\omega t} \\ &= (K_{a1} \underline{F}_1 + K_{a2} \underline{F}_2) e^{j\omega t} \\ &= \underline{F}_a e^{j\omega t}. \end{aligned} \quad (6)$$

Hence, the participation of F_1 and F_2 is equivalent to the participation of a virtual modal force $\underline{F}_a = (K_{a1} \underline{F}_1 + K_{a2} \underline{F}_2)$. In the same way, we define $\underline{F}_b = (K_{b1} \underline{F}_1 + K_{b2} \underline{F}_2)$. This shows the importance of localization of the actuators. Indeed, if they are placed in locations such that $\Phi_a(x_1) = \Phi_a(x_2) = 0$, it becomes impossible to excite the mode a . Of course, the same conclusion holds for mode b . Finally, we introduce the matrix K_{ab} , defined by

$$\begin{pmatrix} \underline{F}_a \\ \underline{F}_b \end{pmatrix} = \begin{pmatrix} \Phi_a(x_1) & \Phi_a(x_2) \\ \Phi_b(x_1) & \Phi_b(x_2) \end{pmatrix} \cdot \begin{pmatrix} \underline{F}_1 \\ \underline{F}_2 \end{pmatrix} = K_{ab} \begin{pmatrix} \underline{F}_1 \\ \underline{F}_2 \end{pmatrix}. \quad (7)$$

According to these definitions, (5) is then revised into

$$m_a \underline{\ddot{w}}_a + d_{sa} \underline{\dot{w}}_a + c_a \underline{w}_a = \underline{F}_a e^{j\omega t}. \quad (8)$$

In the same way, we obtain for the mode b

$$m_b \underline{\ddot{w}}_b + d_{sb} \underline{\dot{w}}_b + c_b \underline{w}_b = \underline{F}_b e^{j\omega t}. \quad (9)$$

Finally, the vibration amplitude for the two modes, and their phase shift, can be calculated using (8) and (9), by

$$\underline{W}_k(t) = \underline{w}_k e^{-j\omega t}. \quad (10)$$

Hence, (6), (8), and (9) describe the evolution of the vibration amplitude for the two modes a and b . These equations yield a model which can be represented by way of a causal ordering graph (COG), as shown in Fig. 7. In principle, only equations using integral relations (ellipses with single arrow) or relations independent of time (ellipses with double arrow) can be used [14]. Hence, the equations are revised into

- $R_K: \underline{F}_k = K_{k1} \underline{F}_1 + K_{k2} \underline{F}_2$,
- $R_\theta: \underline{f}_a = \underline{F}_a e^{j\omega t}, \quad \underline{f}_b = \underline{F}_b e^{j\omega t}$,
- $R_{k1}: \underline{\dot{w}}_k = \frac{1}{m_k} \int (\underline{f}_k - \underline{f}_{ek}) dt$,
- $R_{k2}: \underline{f}_{ek} = c_k \int \underline{\dot{w}}_k dt$,
- $R_\theta^{-1}: \underline{W}_k = \underline{w}_k e^{-j\omega t}$,

with $k \in \{a, b\}$.

To validate the model, we compare in Fig. 8 measurements on the aluminum beam to the model. We compare the actual value of $w(t)$, which is sinusoidal, and the simulated value of the deflection amplitude $W(t)$ which represents the amplitude of $w(t)$ (see Appendix A for a description of the test bench). The measurements on the beam were made with a laser interferometer which measures the vibration speed instead of the deflection. We thus compare $\dot{w}(t)$ for the simulation and the experimental study when $F_2 = 0$ and F_1 is step varying. For the three runs, the experimental conditions were:

- case a: the frequency corresponds to the eigenfrequency of mode a and the step value for $F_1 = 1 N$,

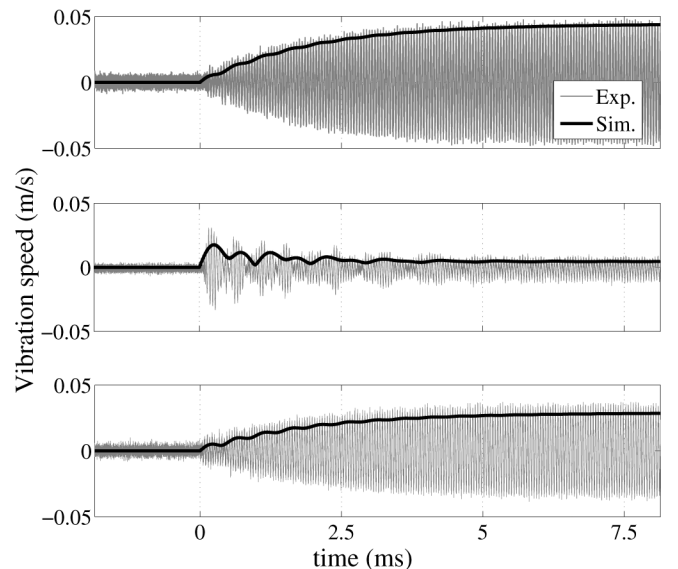


Fig. 8. Comparison between modeling and the experimental output at $x = 0.29$ m.

- case c: the frequency corresponds to the eigenfrequency of mode b and the step value for $F_1 = 1N$,
- case b: the frequency is at the middle of modes a and b , with a step value for $F_1 = 3N$.

The other parameters of simulations are kept constant.

The simulation is found to be consistent with the experimental study, validating the approach. However, this modeling is established in a fixed frame, and state variables are sinusoidal functions of time. However, in this paper, we are interested in the evolution of the deflection amplitude and the phase shift of these variables. This is why, in the next section, the modeling is modified, and presented in a rotating reference frame.

B. Modeling in a Rotating Reference Frame

We have defined \underline{w}_k as two complex numbers. Consequently, \underline{W}_k are the coordinates of \underline{w}_k in a rotating reference frame attached to $e^{j\omega t}$. The rotating reference frame is named (d, q) and is attached to $e^{j\omega t}$ as shown in Fig. 6.

For steady-state operation, \underline{W}_k are constant; hence, the affixes of \underline{w}_k are along a circle in the fixed frame. However, for the most general case, \underline{W}_k depend on time and the positions of their affix vary in the rotating frame.

The purpose of this section is to obtain the dynamic of \underline{W}_k directly, without calculating \underline{w}_k for the general case. We first calculate each derivative of \underline{w}_k :

$$\frac{d\underline{w}_k}{dt} = (j\omega\underline{W}_k + \dot{\underline{W}}_k)e^{j\omega t}, \quad (11)$$

and

$$\frac{d^2\underline{w}_k}{dt^2} = (-\omega^2\underline{W}_k + 2j\omega\dot{\underline{W}}_k + \ddot{\underline{W}}_k)e^{j\omega t}. \quad (12)$$

Substituting (11) and (12) into (8) leads to

$$m_a\ddot{\underline{W}}_a + (d_{sa} + 2m_a j\omega)\dot{\underline{W}}_a + [(c_a - m_a\omega^2) + j\omega d_{sa}]\underline{W}_a = K_a \underline{F}_a, \quad (13)$$

where we also simplified left and right by $e^{j\omega t}$. This equation is linear and can be solved, because ω is constant. However, for the sake of simplification, we make the assumption that $|\dot{\underline{W}}_a| \ll \omega|\underline{W}_a|$ and $|\ddot{\underline{W}}_a| \ll \omega|\dot{\underline{W}}_a|$; this can be acceptable if the dynamic of \underline{W}_a is limited by ω . Then, the terms $d_{sa}\dot{\underline{W}}_a$ and $m_a\ddot{\underline{W}}_a$ can be neglected, compared with $d_{sa}\omega\underline{W}_a$ and $m_a\omega\dot{\underline{W}}_a$, respectively. One consequence is that the closed-loop dynamic proposed in this paper will have to be tempered to fulfill this condition. Finally, (13) can be simplified into

$$2m_a j\omega\dot{\underline{W}}_a + [(c_a - m_a\omega^2) + j\omega d_{sa}]\underline{W}_a = K_a \underline{F}_a. \quad (14)$$

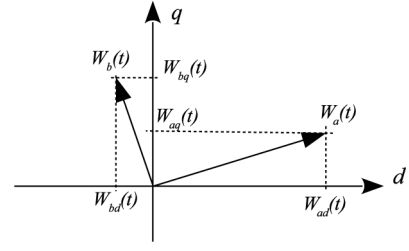


Fig. 9. Representation in a rotating reference frame.

We now project (14) onto axes d and q of the rotating frame. For that purpose, we define $\underline{W}_a = W_{ad} + jW_{aq}$, and $\underline{F}_a = F_{ad} + jF_{aq}$, as illustrated in Fig. 9.

Moreover, we separate the imaginary part and the real part of this equation, leading to two new equations:

$$-2m_a\omega\dot{W}_{aq} - d_{sa}\omega W_{aq} = F_{ad} - (c_a - m_a\omega^2)W_{ad} \quad (15)$$

$$2m_a\omega\dot{W}_{ad} + d_{sa}\omega W_{ad} = F_{aq} - (c_a - m_a\omega^2)W_{aq}. \quad (16)$$

As can be seen, this model can be explained as follows:

- F_{ad} controls W_{aq} , and W_{ad} produces a perturbation,
- F_{aq} controls W_{ad} , and W_{aq} produces a perturbation.

Moreover, for steady state operations, $\dot{W}_{aq} = 0$ and $\dot{W}_{ad} = 0$, and hence, F_{ad} and F_{aq} are constant over time.

A new COG is drawn in Fig. 10, where R_{ad} refers to (15) and R_{aq} to (16). We also represented the equation for mode b , R_{bd} and R_{bq} being given for similar equations.

This model is then compared with simulation in Fig. 11 for a step variation of F_1 from 0 N to 3 N. We have chosen the frequency corresponding to mode a , and then to mode b ; indeed, for these frequencies, the cross-coupling between axes d and q is removed, yielding a first-order type response to step variation of the forces. This is clearly confirmed by the experimental test, which shows responses close to the model.

The advantage of this model is to use variables which are constant at steady state, and not sinusoidal functions of time. This makes the control easier, and we can now devise controls imposing the amplitude and phase of the two modes a and b . The next section presents such a control.

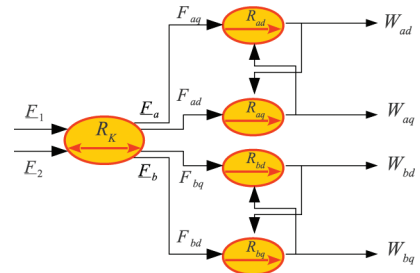


Fig. 10. Causal ordering graph in the rotating reference frame.

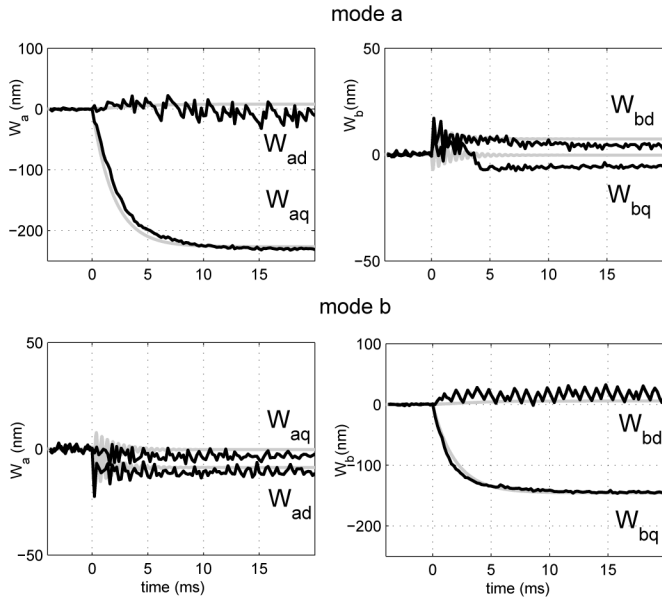


Fig. 11. Simulation (light) compared with experiment (bold), in the case of step variation of F_1 from 0 N to 3 N, at the frequency of mode a (top) and mode b (bottom).

IV. CONTROL OF THE TRAVELING WAVE

A. Control of \underline{W}_a and \underline{W}_b

The working frequency is fixed, and chosen between the eigenfrequency of the two modes. We must control F_{kd} and F_{kq} to obtain

$$\underline{W}_{aref} = j\underline{W}_{bref} \quad (17)$$

automatically. In this way, no optimization loop is necessary at this point to obtain the traveling wave. Hence, the four vibration amplitudes must be controlled.

First, we choose to align the rotating frame on mode a . This condition leads to $W_{adref} = 0$ and $W_{aqref} = W$, and also $W_{bdref} = W$ and $W_{bqref} = 0$. The position of the amplitude reference can be represented in the rotating reference frame, as depicted in Fig. 12.

Four control loops are needed, two for mode a (axes d and q), and two for mode b (axes d and q also). Integral-proportional controllers are used. The decoupling of the two axes is achieved by imposing very different settling times: the dynamics of W_{bd} and W_{aq} are set faster com-

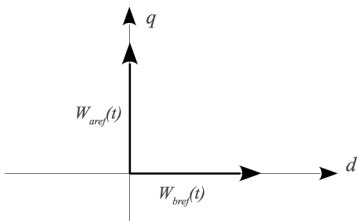


Fig. 12. Amplitude references for modes a and b in the rotating reference frame.

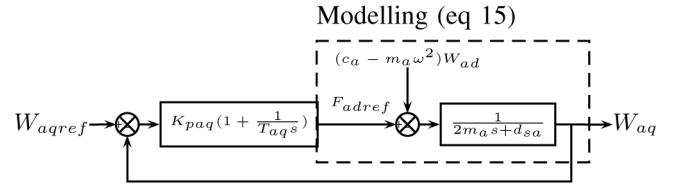


Fig. 13. Closed-loop control for axis q of mode a .

pared with the dynamics of W_{aq} and W_{bd} , respectively, to align the vectors \underline{W}_a and \underline{W}_b on their axes.

The closed-loop control of mode a is thus represented in Fig. 13, and for purpose of illustration, we give in (18) the computation of the force F_{aqref} for the amplitude reference along axis q of mode a , W_{aqref} with s the Laplace variable:

$$F_{daqref} = K_{paq} \left(1 + \frac{1}{T_{aq}s} \right) (W_{aqref} - W_{aq}). \quad (18)$$

Finally, the input forces F_1 and F_2 are calculated using (7), giving:

$$\begin{pmatrix} F_1 \\ F_2 \end{pmatrix} = (K_{ab})^{-1} \begin{pmatrix} F_{adref} + jF_{aqref} \\ F_{bdref} + jF_{bqref} \end{pmatrix}. \quad (19)$$

B. Experimental Results of the Control of Modes a and b

For the beam under study, we have chosen the mode a at $f = 17900$ Hz and the mode b at $f = 20200$ Hz. We have fixed the working frequency in the middle of the eigenfrequencies of mode a and mode b , which is $f = 19050$ Hz. We then applied a step variation of W_{aqref} while the other variables are kept constant and equal to 0. We recorded the variation of the vibration amplitude, as well as the forces \underline{F}_a and \underline{F}_b . The results are presented in Fig. 14.

The results show a closed-loop response time of 250 ms for W_{aq} , which will be also the settling time of the traveling wave. Moreover, we can see how axis d and axis q are

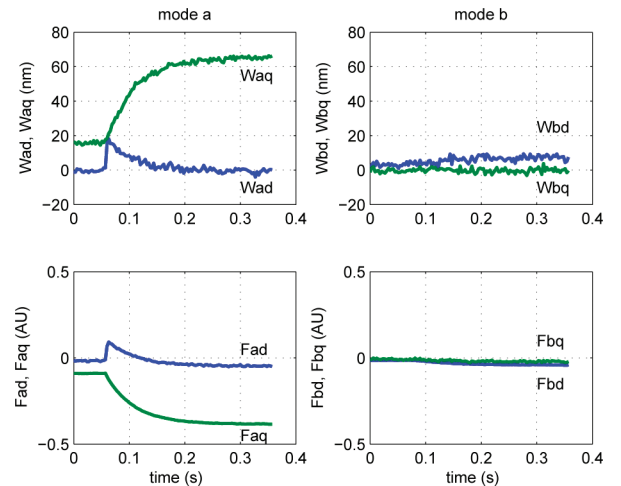


Fig. 14. Transient response to step variation of W_{aqref} from 20 nm to 70 nm.

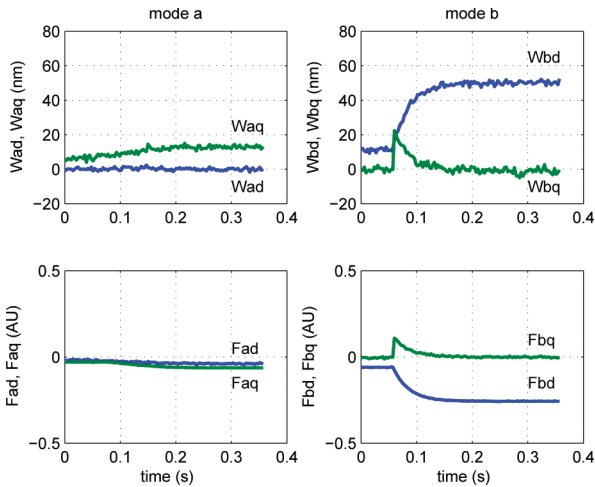


Fig. 15. Transient response to step variation of $W_{b\text{def}}$ from 10 nm to 50 nm.

coupled, because variation of W_{aq} produces a variation of W_{ad} immediately. The corrector of axis d detects this variation, and changes F_{aq} to compensate for the coupling produced by axis q . After 100 ms, W_{ad} returns to 0, and \underline{W}_a is then aligned on axis q again. Mode b is not affected by these changes, which is a consequence of the decoupling of the modes through the use of forces F_a and F_b , as shown by the graph of Fig. 10.

We also present the same trial for mode b in Fig. 15, showing a similar behavior.

C. Experimental Results of the Control of the Traveling Wave in Steady-State

We now control \underline{W}_a and \underline{W}_b to obtain a traveling wave. We conducted two test runs, each at a different frequency. For the first test run, we have chosen $f = 19050$ Hz, which is exactly in the middle between the two modes. For the other one, we have chosen $f = 19200$ Hz, a value closer to the mode b , to check whether or not a traveling wave could be obtained. The results for the two frequency conditions are presented in the space-time plane in Fig. 16, and in the rotating reference frame in Fig. 17.

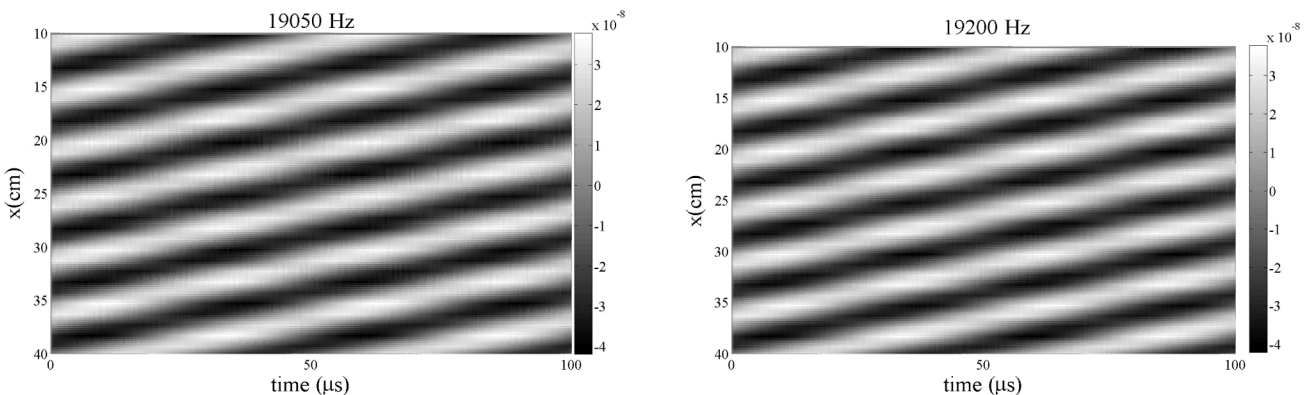


Fig. 16. Deflection as a function of time and space for the two frequency conditions (interpolated).

For each test run, the vibration amplitude of each mode is placed on the right axis, and the condition $\underline{W}_a = j\underline{W}_b$ is fulfilled. The forces F_a and F_b must be adapted to obtain this condition. For $f = 19050$ Hz, this condition results in two modal forces with almost the same amplitude, and phase shifted by approximately $\pi/2$, leading to $\underline{F}_a \simeq j\underline{F}_b$. We can note here that this does not lead to $\underline{F}_1 = j\underline{F}_2$ necessarily; indeed, we obtained for this run $\underline{F}_1 = -0.23 + 0.18j$ and $\underline{F}_2 = 0.15 + 0.14j$. This is due to the matrix K_{ab}^{-1} , which combines the two modal forces to obtain the forces to apply on the beam. Hence, the forces to apply on the beam to obtain a traveling wave depend on the location of the exciters, which modifies K_{ab} . This conclusion is found to be consistent with [10].

For $f = 19200$ Hz, the operating point is closer to mode b , and farther to mode a . The two modal forces \underline{F}_a and \underline{F}_b must adapt to these new conditions: F_a must increase because the participation of the mode a decreases for frequencies above its eigenfrequency, as shown in Fig. 4. This is automatically obtained thanks to the control of W_{ab} . Consequently, with this method, the control automatically adapts the two exciters' supply to obtain the traveling wave, through a closed-loop control which responds in 250 ms.

We then measured the deflection at several positions on the beam to estimate the SWR. Measurements were carried out over 30 cm in the middle of the beam, and a spline interpolation was made between the measurements. The results are presented in Fig. 18.

Hence, the traveling wave is not perfect, despite the condition $\underline{W}_a = j\underline{W}_b$. To decompose the motion into the traveling and standing components, [15] proposes to fit the measured complex amplitude by an ellipse. With this method, we found $\text{SWR} = 1.27$ at $f = 19050$ Hz and $\text{SWR} = 1.30$ at $f = 19200$ Hz. A perfect traveling wave would result in $\text{SWR} = 1.0$. These higher values obtained in our case can be due to several reasons.

For instance, the condition $\underline{W}_a = j\underline{W}_b$ could be badly set, but Fig. 17 shows that is not the case thanks to the control loop.

Still, the values of W_a and W_b could be badly estimated in our test bench. In this case, although the control per-

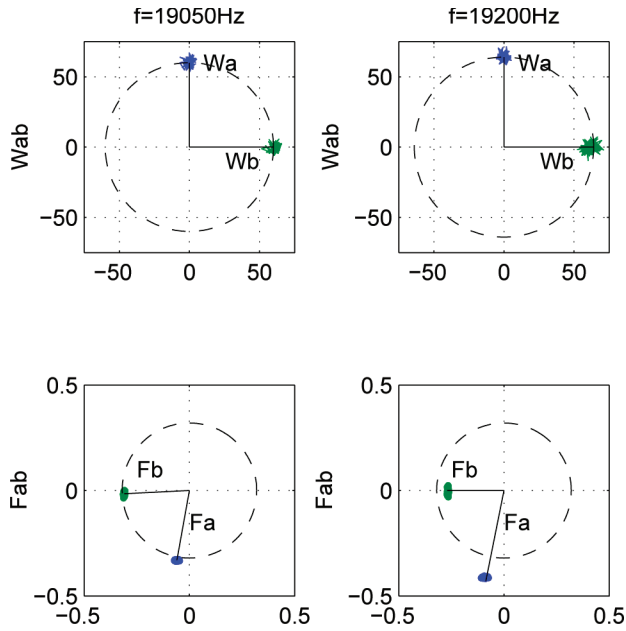


Fig. 17. Diagram in the rotating reference frame of the vibration amplitude and the forces for two frequency conditions.

forms correctly in the rotating frame, a steady-state error would remain in the fixed frame. Another explanation is that, for this operating point, the modes higher than mode b may have a negative influence on the SWR. However, we note that the SWR is not improved, nor increased when changing the frequency. Indeed, changing the frequency also changes the repartition of the modes above b .

In this paper, we settle for the values of SWR experimentally found, and we do not try to obtain a better SWR, which would lead us to modify the position of the exciters, as shown in [9] and [10]. We note, however, that despite the change in frequency, the SWR of the traveling wave is found to be almost constant for the two runs. Hence, the method allows a traveling wave to be obtained at different frequency conditions, as shown in Fig. 16, which presents the deflection measured with a laser interferometer as a function of time and the position. The two figures are very similar.

We have presented our results on steady-state operations, and we have shown that the control can adapt to different conditions of frequency without changing the SWR. The next section of the paper deals with the transient response of the control.

D. Direction Change of the Traveling Wave

Opposite direction of the traveling wave can be obtained by setting an opposite value for \underline{W}_{aref} or \underline{W}_{bref} . This is experimentally checked and presented in Fig. 19, when $W_{bref} = -W_{bref}$.

This figure shows the transient response time; we can observe that a direction reversal is obtained in 150 ms. We also show the trajectory in the rotating reference frame of the vectors \underline{W}_a and \underline{W}_b ; \underline{W}_a is not affected by the direction change, because only W_{bref} is reversed. Moreover, at the end of the direction change, the two vectors are in quadrature.

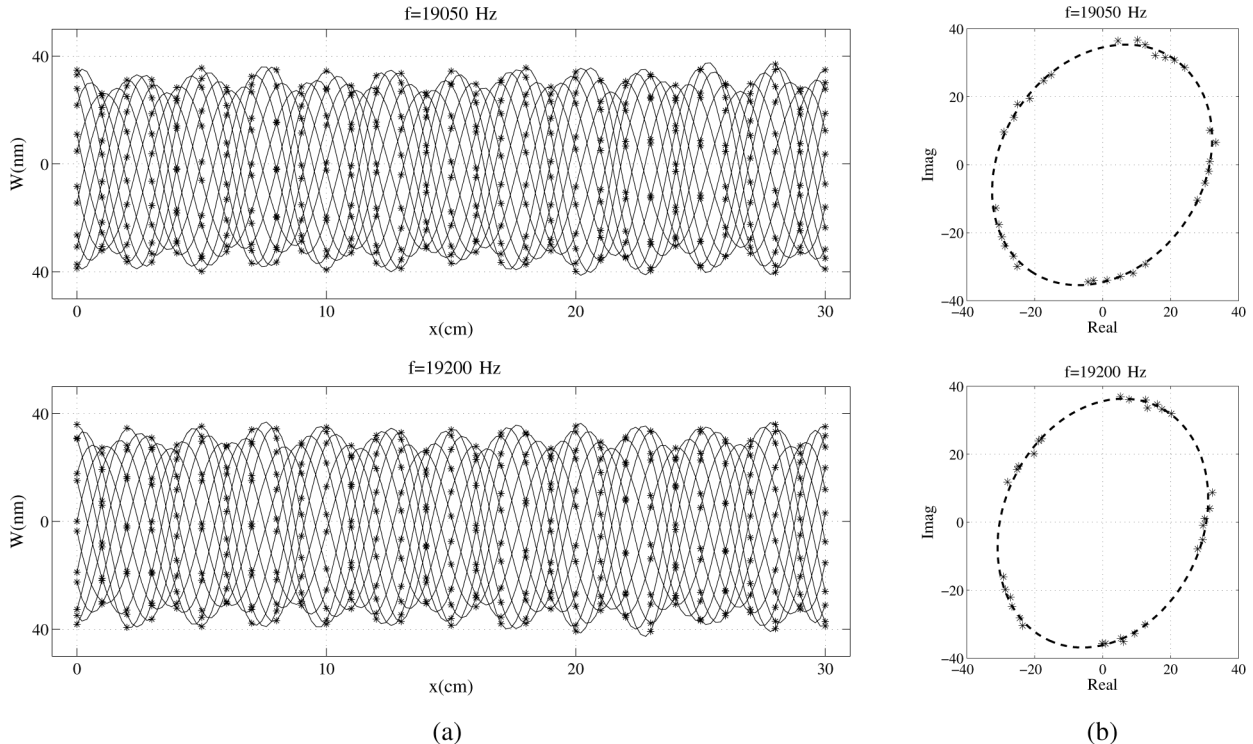


Fig. 18. (a) Deflection as a function of space and for 15 different instants (interpolated) (b) complex deflection and the fitted ellipses; stars represent the actual measurements.

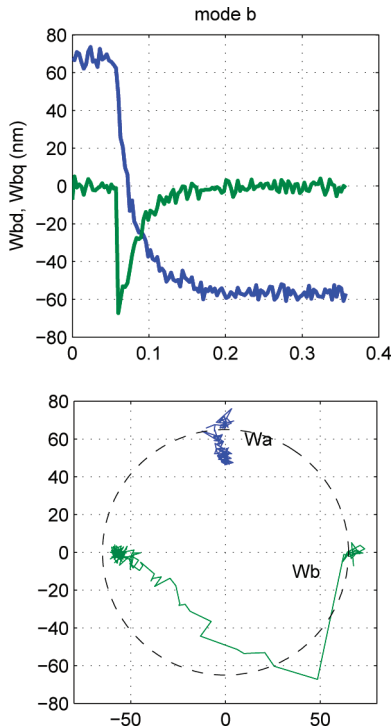


Fig. 19. Direction change of the traveling wave at $t = 0.02$ s.

E. Frequency Change of the Traveling Wave

In this test run, we test whether the method is robust regarding frequency changes. For that purpose, at $t = 0.05$ s, the frequency of the traveling wave is changed from $f = 18500$ Hz to $f = 19500$ Hz. The results presented in Figs. 20 and 21 show no unstable behavior: the deformation amplitude of modes a and b return to their reference values after the perturbation. Mode b is clearly more sensitive to this perturbation. This may be due to the fact that in this run, the frequency reaches a value which is very close to the resonant frequency of mode b : the modal forces must adapt accordingly.

V. CONCLUSION

This paper presents a vector control of two vibration modes to obtain a traveling wave in the middle of a rect-

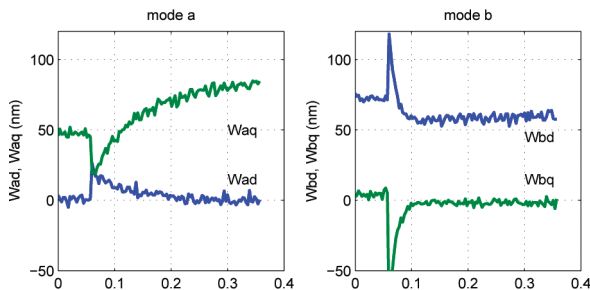


Fig. 20. Transient response of the vibration amplitude to a frequency change $f = 18500$ Hz to $f = 19500$ Hz.

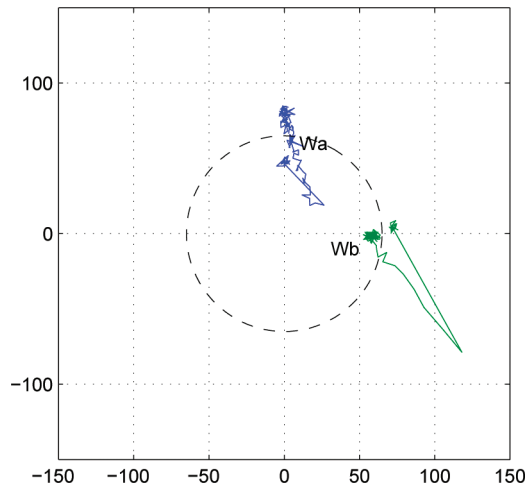


Fig. 21. Response of the system in the rotating reference frame to a frequency change from $f = 18500$ Hz to $f = 19500$ Hz.

angular beam. For that purpose, a specific model in a rotating reference frame is established. In this reference frame, the vibration amplitudes of the two modes are represented by vectors whose magnitudes are the vibration amplitudes, and the angular position is the associated phase. A validation of this model was proposed by comparison with experimental runs.

Then, a control based on this model was presented. It was used to control the magnitude and the phase of the vibration amplitude of the two modes to obtain the traveling wave. We obtained an SWR of 1.3 for two frequency conditions. This result was obtained over 31 cm in the middle of the beam, corresponding to approximately 66% of the total length. Dynamic responses to direction or frequency change were also presented. The advantage of the method is that it doesn't need an optimization loop to tune the excitation parameters of the actuators, which leads to a dynamic behavior.

This result was obtained by controlling two modes only, which are measured in the middle of the beam, where the higher modes have less influence. On one hand, this clearly changes compared with some authors' conclusions, which advise optimization of the participation of up to ten modes. On other the hand, we measured the same SWR for two frequencies, and then with other participation of the higher modes, showing that for the studied beam, these higher modes don't have a strong influence. This is why we think that the proposed method can produce a traveling wave on other beams, but with non-optimized SWR. Further work should clarify this point.

APPENDIX A
THE EXPERIMENTAL TEST BENCH

The experimental verification was carried out using the experimental test bench of Fig. 22. The constitutive elements of the test bench are shown in Fig. 23. The beam used in this experiment is a 6×6 mm square beam with

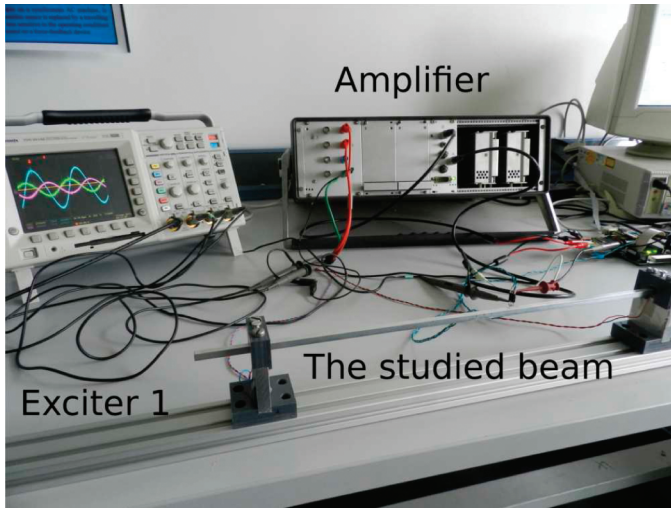



Fig. 22. Experimental test bench showing the studied beam, the exciters and the voltage amplifier. 

$L = 493$ mm. Two piezoelectric actuators are used to excite the beam. We used two multistack actuators (CMAP, Noliac, Kvistgaard, Denmark). These actuators have a low rated voltage (about 30 V) and a resonating frequency well above our working frequency (700 kHz). Thus, we consider that the forces F_1 and F_2 are directly proportional to the supply voltages applied to the piezoelectric actuators named V_1 and V_2 . The actuators are clamped

on the beam by using two specific clamps. The actuators are supplied by two linear amplifiers.

A DSP f2812 (Texas Instruments Inc., Dallas, TX) equipped with a digital-to-analog converter produces the voltage references to the amplifiers. In the DSP, a direct frequency synthesizer is running, and produces two signals proportional to $r(t) = \cos(\omega t)$ and $i(t) = \sin(\omega t)$. These two signals are then multiplied by the real and imaginary parts, respectively, of \underline{F}_1 . The same computation is also achieved for \underline{F}_2 . Hence, it is possible to not only synchronize the forces F_1 and F_2 , but we can also impose their real and imaginary parts.

We also measure the deformation amplitude at specific points x_A and x_B with piezoelectric patches bonded on the beam. These patches are used as sensors because the voltage they produce is directly proportional to $w(x, t)$. The analog-to-digital conversion is synchronized on the signals r and i of the synthesizer. This way, we can measure the real and imaginary parts of these signals. A method detailed in the next section is used to deduce \underline{W}_a and \underline{W}_b from these measurements.

Fig. 23 presents an overview of the experimental setup.

Finally, a control GUI made using Matlab (The MathWorks Inc., Natick, MA) was created to easily control the parameters of the DSP. A laser interferometer is used to identify the deformation along the whole beam.

APPENDIX B IDENTIFICATION OF \underline{W}_A AND \underline{W}_B

To achieve the estimation of each mode's vibration amplitude, Riaz and Feeny [16] propose a method based on the proper orthogonal decomposition of the beam by writing a matrix Φ , which is based on the measurement of the displacement at several position and the deformation mode shape. A minimum number of sensors equal to the number of modes to be identified is required.

In this paper, we assume that in the measurements we only have contributions from the two wanted modes a and b , the others being negligible. We then need two sensors, which are piezo patches located at $x = x_A$ and $x = x_B$. Hence, we can write:

$$\underline{W}_m(x_m, t) = \underline{W}_a \Phi_a(x_m) e^{j\omega t} + \underline{W}_b \Phi_b(x_m), \quad (20)$$

where $m = \{A, B\}$. This yields

$$\begin{pmatrix} \underline{W}_1 \\ \underline{W}_2 \end{pmatrix} = \Phi_{AB} \cdot \begin{pmatrix} \underline{W}_a \\ \underline{W}_b \end{pmatrix}, \quad (21)$$

where

$$\Phi_{AB} = \begin{pmatrix} \Phi_a(x_A) & \Phi_b(x_A) \\ \Phi_a(x_B) & \Phi_b(x_B) \end{pmatrix}. \quad (22)$$

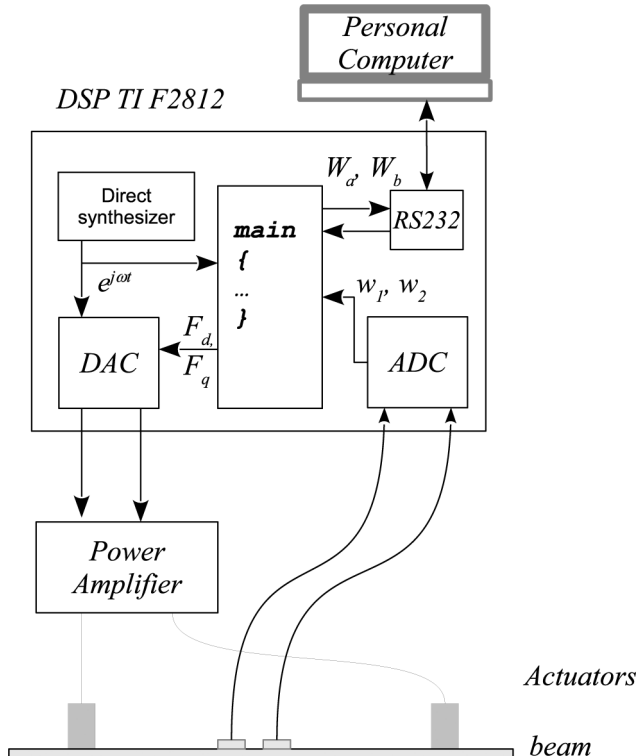


Fig. 23. Architecture of the experimental setup.

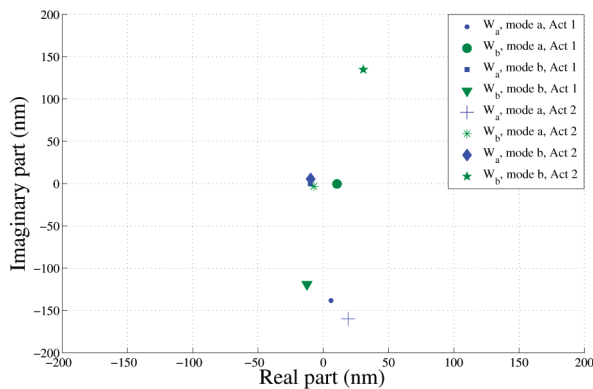



Fig. 24. Identification of \underline{W}_a and \underline{W}_b for several working conditions, in the complex plane; each point represents the mean values calculated over 100 measurements. 

We then choose to place the sensors in positions such that Φ_{AB} is nonsingular. Then, it is possible to calculate the two contributions of each mode, by

$$\begin{pmatrix} \underline{W}_a \\ \underline{W}_b \end{pmatrix} = \Phi_{AB}^{-1} \cdot \begin{pmatrix} \underline{W}_1 \\ \underline{W}_2 \end{pmatrix}. \quad (23)$$

Hence, the identification of \underline{W}_a and \underline{W}_b can be obtained from the measurements of the deformations at x_A and x_B given the deformation mode shapes $\Phi(x)$ at each position.

In Fig. 24, we present the results of the estimation. For that test, we choose two working frequencies to obtain modes a and b successively. We also chose to supply actuator 1 or 2 independently.

From this figure, we can see that when we supply the actuators at the resonance of mode a , then we have \underline{W}_b which is very small compared with \underline{W}_a and vice versa. Moreover, when we compare the cases where $F_2 = 0$ to the cases where $F_1 = 0$, we obtain two results symmetrical for \underline{W}_b , while they are almost concentrated for \underline{W}_a . This is due to the fact that mode a is a symmetric mode, and thus $\Phi_a(x_1) = \Phi_a(x_2)$ (because we chose $x_2 = L - x_1$), and thus $K_{a1} = K_{a2}$, whereas mode b is antisymmetric, leading to $K_{b1} = -K_{b2}$. The results found are thus consistent with the theory, and we have a way to identify the deformation amplitude for each mode.

REFERENCES

- [1] S. Ueha, Y. Tomikawa, M. Kurosawa, and N. Nakamura, *Ultrasonic Motors: Theory and Applications*. Oxford, UK: Clarendon Press, 1993.
- [2] B.-G. Loh and P. I. Ro “An object transport system using flexural ultrasonic progressive waves generated by two-mode excitation,” *IEEE Trans. Ultrason. Ferroelectr. Freq. Control*, vol. 47, no. 4, pp. 994–999, 2000.
- [3] X. Li, Y. Sun, C. Chen, and C. Zhao, “Oscillation propagating in non-contact linear piezoelectric ultrasonic levitation transporting system—From solid state to fluid media,” *IEEE Trans. Ultrason. Ferroelectr. Freq. Control*, vol. 57, no. 4, pp. 951–956, 2010.

- [4] S. Miyazaki, T. Kawai, and M. Araragi, “A piezo-electric pump driven by a flexural progressive wave,” in *Proc. IEEE Micro Electro Mechanical Systems*, 1991, pp. 283–288.
- [5] D. Sun, S. Wang, S. Hata, J. Sakurai, and A. Shimokohbe, “Theoretical and experimental investigation of traveling wave propagation on a several-millimeter-long cylindrical pipe driven by piezoelectric ceramic tubes,” *IEEE Trans. Ultrason. Ferroelectr. Freq. Control*, vol. 57, no. 7, pp. 1600–1611, 2010.
- [6] M. Kuribayashi, “Excitation conditions of flexural traveling waves for a reversible ultrasonic linear motor,” *J. Acoust. Soc. Am.*, vol. 77, no. 4, pp. 1431–1435, 1985.
- [7] N. Tanaka and Y. Kikushima, “Active wave control of a flexible beam: Proposition of the active sink method,” *JSME Int. J.*, vol. 34, no. 2, pp. 159–167, Jun. 1991.
- [8] R. Gabai and I. Bucher “Spatial and temporal excitation to generate traveling waves in structures,” *J. Appl. Mech.*, vol. 77, no. 2, art. no. 021010, Dec. 2010.
- [9] B. Dehez, C. Vloebergh, and F. Labrique, “Study and optimization of traveling wave generation in finite-length beams,” *Math. Comput. Simul.*, vol. 81, no. 2, pp. 290–301, Oct. 2010.
- [10] A. Mimikes, R. Gabay, J. Bucher, and M. Feldman, “On the sensing and tuning of progressive structural vibration waves,” *IEEE Trans. Ultrason. Ferroelectr. Freq. Control*, vol. 52, no. 9, pp. 1565–1576, Sep. 2005.
- [11] R. Gabai and I. Bucher “Excitation and sensing of multiple vibrating traveling waves in one-dimensional structures,” *J. Sound Vibrat.*, vol. 319, no. 1–2, pp. 406–425, 2009.
- [12] M. Abu-Hilal, “Forced vibration of Euler–Bernoulli beams by means of dynamic Green functions,” *J. Sound Vibrat.*, vol. 267, no. 2, pp. 191–207, Oct. 2003.
- [13] C. Giraud-Audine and B. Nogarède, “Analytical modelling of travelling-wave piezomotor stators using a variational approach,” *Eur. Phys. J. AP*, vol. 6, no. 1, pp. 71–79, 1999.
- [14] F. Giraud and B. Semail, “A torque estimator for a traveling wave ultrasonic motor—Application to an active claw,” *IEEE Trans. Ultrason. Ferroelectr. Freq. Control*, vol. 53, no. 8, pp. 1468–1477, 2006.
- [15] I. Bucher, “Estimating the ratio between travelling and standing vibration waves under non-stationary conditions,” *J. Sound Vibrat.*, vol. 270, no. 1–2, pp. 341–359, 2004.
- [16] M. S. Riaz and B. F. Feeny, “Proper orthogonal modes of a beam sensed with strain gages,” *J. Vib. Acoust.*, vol. 125, no. 1, pp. 129–131, Jan. 2003.



Frédéric Giraud received the B.S. degree in 1995 from Paris-XI University, graduated from the Ecole Normale Supérieure de Cachan, France in 1996 in electrical engineering, and received the M.S. degree in 1997 from the Institut National Polytechnique de Toulouse and the Ph.D. degree in 2002 from the University Lille 1. He is a member of the electrical engineering and power electronics laboratory of Lille, where he works as an Associate Professor. His research deals with the modeling and control of piezoelectric actuators.



Christophe Giraud-Audine received his M. Eng. degree in mechanical engineering from the École Nationale Supérieure d’Arts et Métiers in 1992 and his Ph.D. degree in electrical engineering from the Institut National Polytechnique de Toulouse in 1998. After two years spent as a Research Associate at the University of Sheffield, he took an Associate Professor position at the École Nationale Supérieure d’Arts et Métiers. His current research focuses on the modeling and control of devices based on piezoelectric and shape memory alloys.



Michel Amberg has been teaching electronics at the University of Lille, France. He graduated from the Ecole Normale Supérieure de Cachan, France in 1981. He has tutored more than a hundred bachelor's students during their projects in the field of telecommunications, computer science, and electronics. He is now a research engineer at IRCICA, and works on the electronic design of tactile devices.



Betty Lemaire-Semail received the Ph.D. degree in 1990 from the University of Paris XI, Orsay. From 1990 to 1998, she was an assistant professor at the Ecole Centrale of Lille and she is now a professor at the University Lille 1. She is a member of the electrical engineering and power electronics laboratory of Lille and head of the research axis on the control of electrical systems. She has studied electromagnetic motors, and her main field of interest now deals with the modeling and control of piezoelectric actuators for positioning and force feedback applications.